Dielectric-based extremely-low-loss subwavelength-light transport at the nanoscale: An alternative to surface-plasmon-mediated waveguiding

Junjie Du,[1,2,4] Shiyang Liu,[1,2,*] Zhifang Lin,[2,3] Jian Zi,[3,2] and S. T. Chui[4]

[1]*Institute of Information Optics, Zhejiang Normal University, Jinhua, Zhejiang 321004, China*

[2]*State Key Laboratory of Surface Physics and Department of Physics, Fudan University, Shanghai 200433, China*

[3]*Key Laboratory of Micro and Nano Photonic Structures (Ministry of Education), Fudan University, Shanghai 200433, China*

[4]*Bartol Research Institute, University of Delaware, Newark, Delaware 19716, USA*

(Received 10 November 2010; published 14 March 2011)

It is demonstrated that with appropriately arranged dielectric nanoparticle structures an extremely low loss guiding of light is achievable at the nanoscale. These dielectric nanoparticle waveguides (DNPWs) exhibit subwavelength transverse confinement of light comparable with metallic plasmon particle waveguides (MPPWs). Different from the MPPWs subject to inevitable intrinsic absorption loss, the material loss for some DNPWs is negligible, enabling long-distance light transport and offering an alternative choice for integrated photonics.

DOI: 10.1103/PhysRevA.83.035803 PACS number(s): 42.79.Gn, 42.82.−m, 73.20.Mf

Nanoscale ultrafast transistors have become the main elements in current chip-scale technology, but the speed of information transport between transistors is much slower than that in transistors in conventional electronic interconnects, greatly limiting the data processing capability of the whole chip. Plasmonics employs the unique optical properties of the surface plasmon resonance occurring at the metal-dielectric interface to confine the electromagnetic (EM) energy, enabling the guiding and manipulating of optical signal at scales much smaller than its wavelength. Metallic plasmon-based interconnects have therefore been proposed as a candidate for fast signal transport between transistors [1–3]. Several configurations, such as band-gap waveguides, metal strips, gap waveguides, groove waveguides, nanowire waveguides, and metallic plasmon particle waveguides (MPPWs), have been designed to guide the EM energy [4–8]. Therein, MPPWs exhibit excellent lateral confinement and appear to be the most promising candidate to match nanoscale transistors. However, the corresponding propagation length is usually below the requirement for practical applications. The main reason for this trade-off between the transverse mode size and the propagation distance originates from the intrinsic material loss of the metal.

As a result, several other schemes have been designed to reduce the intrinsic absorption and realize the long-range propagation. Among others, a hybrid plasmonic waveguide composed of a high-index dielectric wire arranged near a metal surface was proposed and exhibits better propagation distance [9]. Dielectric wire waveguides [10–12] were investigated as well and low-loss light energy propagation was demonstrated. Guiding light energy with a dielectric particle chain has been explored using the whispering-gallery modes of particles, but light energy was not transferred on the subwavelength scale [13]. Although highly desirable for the purpose of miniaturization, nanoscale dielectric particle arrays serving as waveguides with subwavelength lateral confinement remain unexplored, partially due to the higher requirement for the materials ($\varepsilon > 14$). In this Brief Report, our effort is devoted to the investigation of light transport behaviors of the nanoscale dielectric particle-based photonic circuit elements. An extremely low-loss light propagation with excellent transverse confinement comparable with MPPWs is demonstrated in straight chain, corner, and Y-junction configurations under realistic circuit conditions.

For the convenience of analysis, we first demonstrate the light transport behaviors of an MPPW. Figure 1 illustrates the propagation of light along a typical MPPW consisting of a chain of 90 Ag spherical particles along the x direction. The particle has a radius $r = 50$ nm and the particle separation is $a_0 = 150$ nm. The simulation is performed with the rigorous multiple scattering method [14]. The permittivity of Ag particles is described by a Drude model of the form $\varepsilon = \varepsilon_h - (\varepsilon_s - \varepsilon_h)\omega_p^2/(\omega^2 + i\gamma\omega)$ with $\varepsilon_h = 5.45$, $\varepsilon_s = 6.18$, $\omega_p = 1.72 \times 10^{16}$ Hz, and $\gamma = 8.35 \times 10^{13}$ Hz [15]. Figures 3(d) and 3(e) display the electric field intensity patterns in two characteristic planes passing through the chain axis for the case without considering the intrinsic material loss (by setting $\gamma = 0$). It can be seen that the light energy is efficiently transferred along the chain for a Gaussian beam incident along the y axis, polarized along the $z$axis, and focused at the first spherical particle. The corresponding wavelength is $\lambda = 430$ nm and the numerical aperture is NA $= 0.9$. The transverse confinement of the MPPW is measured by calculating the full width at half maximum (FWHM) of the electric field intensity as shown in Figs. 1(d) and 1(e) along some typical lateral lines. It can be seen that the FWHM is about 120 nm and the light energy is strongly confined to the surface of the spherical particles. However, although silver is the metal with nearly the lowest material absorption in the optical frequency range, the realistic damping (with $\gamma = 8.35 \times 10^{13}$ Hz) still substantially attenuates the light transport, leading to a decay rate of about 0.2 dB per 100 nm. This is illustrated in Fig. 1(c). Some other research indicates even more severe loss (about 0.6 dB per 100 nm) [16,17]. However, a comparison of Figs. 1(b) and 1(c) suggests that the usage of materials with sufficiently low material loss might be a promising route to achieve long-range propagation while keeping the strong subwavelength confinement.

Along this line, we examine the feasibility of realizing long-range light guiding by replacing the metallic particles

*syliu@fudan.edu.cn

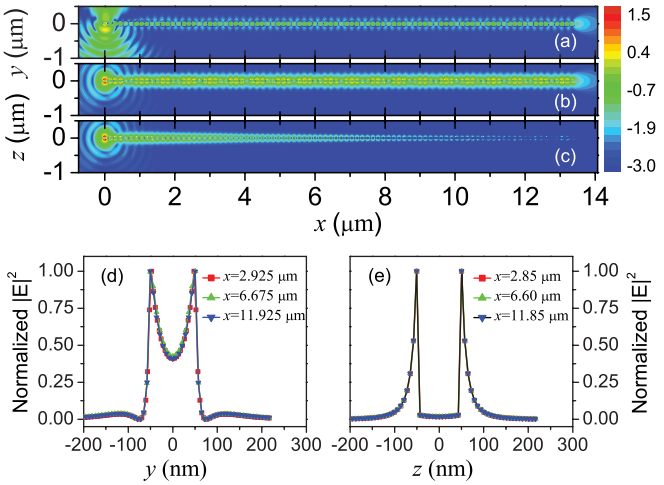

FIG. 1. (Color online) The electric field intensity pattern (in logarithmic scale) near a metallic chain consisting of 90 Ag spherical particles for $\gamma = 0$ (a) in the x-y plane, (b) in the x-z plane, and (c) $\gamma \neq 0$ in the x-z plane. Normalized electric field intensity along some typical lateral lines passing through (d) voids between Ag particles and (e) Ag particle centers.

in an MPPW with dielectric ones, but without sacrificing the lateral confinement. As shown in Fig. 1, the localized surface plasmon resonance (LSPR) supported by metallic particles is physically a kind of subwavelength resonance, in the sense that the resonant wavelength in the host medium is several times bigger than the particle size. Near the LSPR, the strong EM coupling between adjacent particles suppresses the outgoing radiation, resulting in the formation of the guiding mode in an MPPW. From the aspect of the dispersion relation, the guiding modes manifest themselves as a photonic band below the light line, as shown by the (red) dashed line in Fig. 2(a), obtained with the rigorous multiple scattering theory for an infinite spherical particle chain. From Mie scattering theory, it is known that high-index dielectric particles can exhibit a subwavelength resonance as well. Accordingly, we can expect a similar guiding mode mediated by a chain of high-index dielectric particles, as corroborated first by the dispersion curve [solid (blue) line] shown in Fig. 2(a). In the calculation, the permittivity of the spherical dielectric particle is taken as $\varepsilon_s = 15.5$, and the particle size and interparticle separation

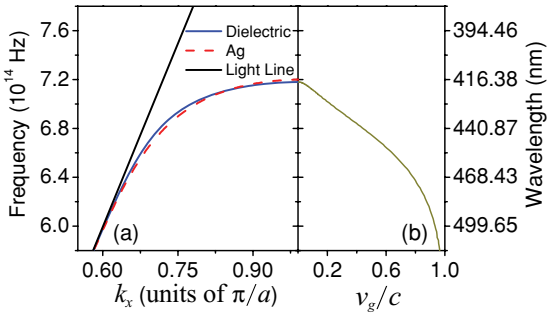

FIG. 2. (Color online) (a) Dispersion curves of an infinite chain of spherical Ag and dielectric particles. (b) Group velocity v_g vs wavelength for the dielectric particle chain. The spherical particle radius and the interparticle separation are the same as those in Fig. 1.

are the same as those for the Ag nanoparticle chain. The remarkable similarity of the photonic bands for the Ag and dielectric particle chains suggests the possibility of guiding the light wave below the diffraction limit with a high-index dielectric particle array. Due to the negligible material loss of dielectrics in the optical range, light energy transport might be achievable with much better performance. In addition, the dielectrics with the real part $\varepsilon_s^{(1)}$ of the permittivity big enough (>14) and the imaginary part $\varepsilon_s^{(2)}$ negligible in the optical range are available. Some dielectric materials such as Si_xGe_{1-x} for $x = 0.7$, 0.8, or 0.9 are good candidates [18]. In the following, we demonstrate the light guiding behaviors of the dielectric nanoparticle waveguides (DNPWs) at the nanoscale. It can be found that the DNPWs not only exhibit the merit of long-range propagation with nanoscale lateral confinement but also possess the capability of ultrafast information transport, providing an alternative to MPPWs for carrying information in the chip.

Before constructing the DNPWs for light transporting, some remarks are in order. (i) Let $k_\perp$ be the transverse wave vector normal to the propagation direction, approximately $k_\perp = \sqrt{(2\pi/\lambda)^2 - k_x^2}$, with λ the wavelength of the guided wave and k_x the wave vector along the chain. To suppress the radiation loss, $k_\perp$ must be imaginary. (ii) As k_x takes its maximum at the Brillouin zone boundary $K_B = \pi/a_0$ for a particle chain with a_0 being the particle separation, the necessary condition to support a waveguide mode turns out to be [19,20]

$$a_0 < \lambda/2. \tag{1}$$

(iii) Nanoparticles are therefore required to be arranged closely regardless of MPPWs or DNPWs [2,4,8,16]. On the other hand, to avoid overlap, the radius of the particle should satisfy $r < a_0/2$. Conditions (i), (ii), and (iii), together with condition (iv), the condition for the occurrence of the Mie resonance, constitute a requirement for the permittivity of the dielectric particle.

Next, we construct various chain structures composed of dielectric spherical particles with radius $r = 50$ nm and interparticle separation $a_0 = 150$ nm under the realistic circuit condition to guide the light energy. All the configurations meet conditions (i)–(iv) at the working wavelength $\lambda = 430$ nm in order to suppress the radiative loss. These parameters are the same as those for the MPPW shown in Fig. 1 for the purpose of comparison. The spherical particles considered have permittivity $\varepsilon_s = 15.5$ [18]. As can be seen from Fig. 2(b), the group velocity is about $v_g = c/4$ at the working wavelength, close to light speed, ensuring the fast data transporting capability required by the nanoscale integration circuits. All the simulations are performed with the multiple scattering method.

As the first example, we demonstrate the light energy transport for a straight DNPW consisting of 90 dielectric nanoparticles. The DNPW arranged along the x axis is illuminated by a Gaussian beam propagating in the y axis and polarized along the z axis for its electric component. The beam has the unit electric field amplitude at the beam center and the numerical aperture NA = 0.9. It is focused on the spherical particle at the beginning of the chain.

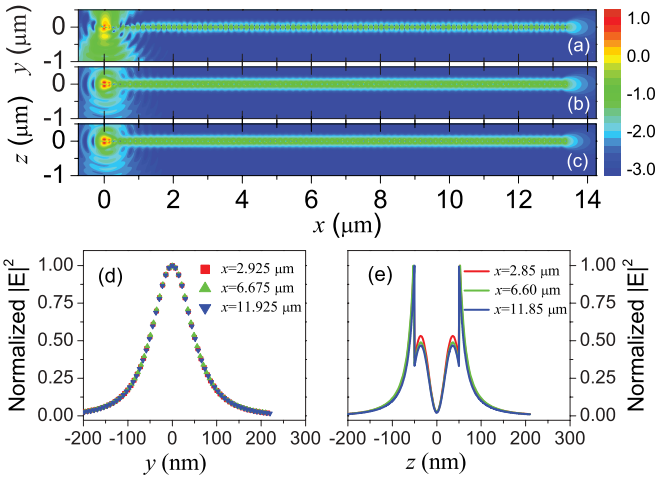

FIG. 3. (Color online) The electric field intensity pattern near a chain consisting of 90 spherical particles with (a) $\varepsilon_s^{(1)} = 15.5$ and $\varepsilon_s^{(2)} = 0$ in the x-y plane, (b) $\varepsilon_s^{(1)} = 15.5$ and $\varepsilon_s^{(2)} = 0$ in the x-z plane, and (c) $\varepsilon_s^{(1)} = 15.5$ and $\varepsilon_s^{(2)} = 0.01$ in the x-z plane. The beam is focused at $x = y = z = 0$, corresponding to the center of the first spherical particle. Normalized electric field intensity along the typical transverse lines (d) between the particles and (e) passing through particle centers are shown.

Figures 3(a) and 3(b) illustrate the electric field intensity patterns of the DNPW in the x-y plane and the x-z plane, respectively, in the logarithmic scale when neglecting the loss (by setting $\varepsilon_s^{(2)} = 0$). The transfer of the optical energy along the DNPW occurs, akin to the MPPW shown in Figs. 1(a) and 1(b). Figure 3(c) presents the field pattern when the loss is taken into account (by setting $\varepsilon^{(2)} = 0.01$, a value much greater than the real material parameter for Si_xGe_{1-x} [18]). Different from the MPPW as shown in Fig. 1(c), the realistic material damping for the DNPW has only a tiny effect on the transport of the light energy, corresponding to a decay length about 0.01 dB per 100 nm. Figures 3(d) and 3(e) display the electric field intensity along some typical lines transverse to the DNPW in the x-y and x-z planes, respectively. It can be found that, when normalized to the maximum value on each line, data for different transverse lines collapse onto a single one, indicating the same transverse confinement at different part of the DNPW. In addition, the FWHM is about 120 nm, suggesting a comparable transverse confinement for the MPPW as shown in Figs. 1(d) and 1(e). With the above analysis, it is obvious that DNPW can serve as an excellent alternative interconnect to implement the high degree of integration in future chip technology.

The transverse confinement also depends on the operating wavelength, as can be seen from Fig. 4(a) for the FWHM along the transverse lines between the particles and through the particle center. The strongest confinement occurs near the band edge and it becomes weaker gradually with the increase of the operating wavelength. The degree of the transverse confinement can also be evaluated by the mode area A_m, which is defined as the ratio of the total mode energy to its peak energy density [9]:

$$A_m = \frac{1}{\max\{W(\mathbf{r})\}} \int_{A_\infty} W(\mathbf{r})\, dA, \qquad (2)$$

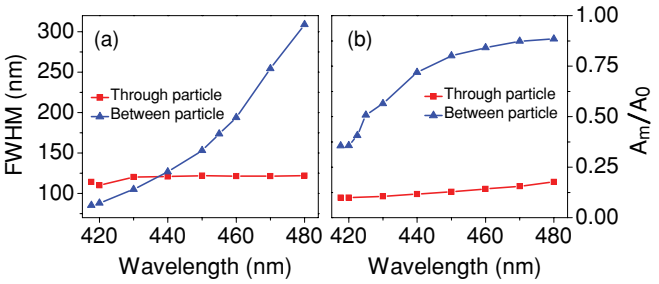

FIG. 4. (Color online) (a) FWHM through particles and between particles and (b) the mode area are plotted as the functions of the working wavelength.

where $W(\mathbf{r}) = \frac{1}{2}\mathrm{Re}\{\frac{\mathrm{d}[\omega\varepsilon(\mathbf{r})]}{\mathrm{d}\omega}|\mathbf{E}(\mathbf{r})|^2\} + \frac{1}{2}\mu_0|\mathbf{H}(\mathbf{r})|^2$ is the energy density, $\varepsilon(\mathbf{r})$ is the permittivity, and μ_0 is the vacuum permeability. The integration is over an area perpendicular to the propagating direction. In Fig. 4(b) we present the mode area normalized by $A_0 = (\lambda/2)^2$ for the integral surfaces passing through the particle center and through the interparticle void. It can be seen that the mode area calculation is consistent with the FWHM results, suggesting the subwavelength transverse confinement in the DNPW from another point of view. It should be pointed out that near the band edge the group velocity is close to zero, resulting in a tiny transport efficiency inappropriate for application in integrated photonics. Accordingly, the operating wavelength chosen in our simulation is located at the mediate position of the photonic band, ensuring the simultaneous achievement of strong confinement and large group velocity.

In the chip technology, interconnects inevitably form corner and Y-junction configurations, but the light energy is still required to continue its propagation after meeting these structures [17]. In this part, we examine the corresponding working efficiency of the DNPWs in such situations. The corner structure is composed of two linear arrays of N_l spherical particles that make a finite angle θ_l. A typical field intensity pattern in logarithmic scale is shown in Fig. 5(a) for a corner structure with $N_l = 45$ and $\theta_l = 45°$, illuminated by a Gaussian beam propagating in the y axis, polarized along the z axis, and focused at the first spherical particle in the horizontal arm. The light is seen to make a turn around the corner. For the Y-junction structure composed of three linear arrays of N_y spherical particles with two forked arrays opening an angle of θ_y, the typical result is shown in Fig. 5(b) for $N_y = 45$ and $\theta_y = 60°$. It can be seen that the light energy propagates along the horizontal main arm first and then splits into two branches at the bifurcation. Due to the big change of the propagation direction at the corner or at the Y junction, some light energy

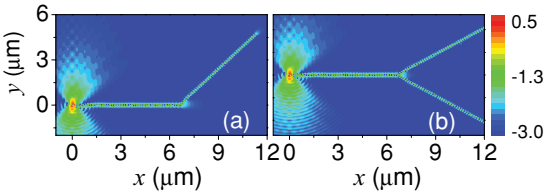

FIG. 5. (Color online) The electric field intensity pattern of the DNPWs with (a) corner and (b) Y-junction configurations.

will be radiated into the far field. Our calculations indicate that the ratio of light energy in the side arm to that in the main arm is about -5 dB for the corner and -2.9 dB for the Y junction for the case shown in Fig. 5. With the increase of θ_l or θ_y, the transport efficiency decreases in the corner or Y-junction structures. Further work is still needed to enhance transport efficiency by, e.g., optimizing the particle radius and separation.

In summary, we have demonstrated the efficient subwavelength transport of light energy at the nanoscale with the use of DNPWs, including guiding light energy along a straight chain, bending light at a corner, and splitting light at a Y junction. Our results suggest that DNPWs can circumvent the inherent restraint in the MPPWs due to the intrinsic material loss without sacrificing the lateral confinement and, therefore, serve as alternative interconnects to realize the long-distance propagation for high-density integrated circuits in the chip technology. Consequently, it can be expected that DNPWs will provide with us a promising scheme to bridge the gap between electronics and photonics at the nanoscale.

This work is supported by the China 973 Program (Grant No. 2006CB921706), NNSFC (Grants No. 10774028 and No. 10904020), MOE of China (Grant No. B06011), SSTC (Grant No. 08dj1400302), ZPNSFC (Grant No. Y1100041), and CPSF (Grant No. 200902211). S. T. Chui is partly supported by the US DOE.

[1] E. Ozbay, Science **311**, 189 (2006).
[2] W. L. Barnes, A. Dereux, and T. W. Ebbesen, Nature (London) **424**, 824 (2003).
[3] R. Zia, J. A. Schuller, A. Chandran, and M. L. Brongersma, Mater. Today **9**, 20 (2006).
[4] S. A. Maier, P. G. Kik, H. A. Atwater, S. Meltzer, E. Harel, B. E. Koel, and A. A. G. Requicha, Nat. Mater. **2**, 229 (2003).
[5] S. I. Bozhevolnyi, J. Erland, K. Leosson, P. M. W. Skovgaard, and J. M. Hvam, Phys. Rev. Lett. **86**, 3008 (2001).
[6] P. Berini, Phys. Rev. B , **61**, 10484 (2000).
[7] J. R. Krenn, B. Lamprecht, and H. Ditlbacher, Europhys. Lett. **60**, 663 (2002); I. V. Novikov and A. A. Maradudin, Phys. Rev. B **66**, 035403 (2002); K. Tanaka and M. Tanaka, Appl. Phys. Lett. **82**, 1158 (2003); D. K. Gramotnev and D. F. P. Pile, *ibid.* **85**, 6323 (2004).
[8] S. A. Maier, *Plasmonics: Fundamental and Applications* (Springer, New York, 2007).
[9] R. F. Oulton, V. J. Sorger, D. A. Genov, D. F. P. Pile, and X. Zhang, Nat. Photon. **2**, 496 (2008).
[10] L. Tong, R. R. Gattass, J. B. Ashcom, S. He, J. Lou, M. Shen, I. Maxwell, and E. Mazur, Nature (London) **426**, 816 (2003).
[11] M. Law, D. J. Sirbuly, J. C. Johnson, J. Goldberger, R. J. Saykally, and P. Yang, Science **305**, 1269 (2004).
[12] C. J. Barrelet, A. B. Grreytak, and C. M. Lieber, Nano Lett. **4**, 1981 (2004); L. K. van Vust, B. Zhang, B. Piccione, A. A. Spector, and R. Agarwal, *ibid.* **9**, 1684 (2009).
[13] Y. Hara, T. Mukaiyama, K. Takeda, and M. Kuwata-Gonokami, Phys. Rev. Lett. **94**, 203905 (2005).
[14] L. M. Li and Z. Q. Zhang, Phys. Rev. B **58**, 9587 (1998); S. Y. Liu and Z. F. Lin, Phys. Rev. E **73**, 066609 (2006); S. Y. Liu, W. K. Chen, J. J. Du, Z. F. Lin, S. T. Chui, and C. T. Chan, Phys. Rev. Lett. **101**, 157407 (2008).
[15] P. G. Kik, S. A. Maier, and H. A. Atwater, Phys. Rev. B **69**, 045418 (2004).
[16] M. Quinten, A. Leitner, J. R. Krenn, and F. R. Aussenegg, Opt. Lett. **23**, 1331 (1998).
[17] S. A. Maier, M. L. Brongersma, P. G. Kik, S. Meltzer, Ari A. G. Requicha, and H. A. Awater, Adv. Mater. **13**, 1501 (2001).
[18] E. D. Palik, *Handbook of Optical Constants of Solids* (Academic, New York, 1998).
[19] A. L. Burin, H. Cao, G. C. Schatz, and M. A. Ratner, J. Opt. Soc. Am. B **21**, 121 (2004).
[20] G. S. Blaustein, M. I. Gozman, O. Samoylova, I. Ya. Polishchuk, and A. L. Burin, Opt. Express **15**, 17380 (2007).